

THE SPECTRUM OF THE EXTRAGALACTIC FAR
INFRARED BACKGROUND FROM THE *COBE*¹ FIRAS
OBSERVATIONS

D.J. Fixsen^{2,3}, E. Dwek⁴, J. C. Mather⁴, C. L. Bennett⁴, and R. A. Shafer⁴

Received _____; accepted _____

Draft printed: August 23, 2018

¹The National Aeronautics and Space Administration/Goddard Space Flight Center (NASA/GSFC) is responsible for the design, development, and operation of the *Cosmic Background Explorer (COBE)*. Scientific guidance is provided by the *COBE* Science Working Group. GSFC is also responsible for the development of the analysis software and for the production of the mission data sets.

²Hughes STX Corporation, Code 685, NASA/GSFC, Greenbelt MD 20771.

³e-mail: fixsen@stars.gsfc.nasa.gov

⁴Laboratory for Astronomy and Solar Physics, Code 685, NASA/GSFC, Greenbelt MD 20771.

ABSTRACT

The *COBE* FIRAS data contain foreground emission from interplanetary, Galactic interstellar dust and extragalactic background emission. We use three different methods to separate the various emission components, and derive the spectrum of the extragalactic Far InfraRed Background (FIRB). Each method relies on a different set of assumptions, which affect the FIRB spectrum in different ways. Despite this, the FIRB spectra derived by these different methods are remarkably similar. The average spectrum that we derive in the $\nu = 5 - 80 \text{ cm}^{-1}$ (2000 -125 μm) frequency interval is: $I(\nu) = (1.3 \pm 0.4) \times 10^{-5} (\nu/\nu_0)^{0.64 \pm .12} P_\nu(18.5 \pm 1.2 \text{ K})$, where $\nu_0 = 100 \text{ cm}^{-1}$ ($\lambda_0 = 100 \mu\text{m}$) and P is the Planck function. The derived FIRB spectrum is consistent with the DIRBE 140 and 240 μm detections. The total intensity received in the 5 - 80 cm^{-1} frequency interval is $14 \text{ nW m}^{-2} \text{ sr}^{-1}$, and comprises about 20% of the total intensity expected from the energy release from nucleosynthesis throughout the history of the universe.

Subject headings: cosmology: Far Infrared background — cosmology: observations

1. INTRODUCTION

The FIRAS (Far Infrared Absolute Spectrophotometer) instrument aboard the Cosmic Background Explorer (*COBE*) satellite (Boggess et al. 1992 and references therein; Mather, Fixsen, & Shafer 1993) was designed to measure the spectrum of the Cosmic Microwave Background (CMB), the Galaxy, and the Far InfraRed Background (FIRB). The FIRAS instrument and calibration are discussed by Mather, Fixsen & Shafer (1993) and Fixsen et al. (1994b). The FIRAS observations of the CMB are discussed by Mather et al. (1990, 1994), and Fixsen et al. (1994a, 1996, 1997a). The FIRAS observations of the Galaxy are discussed in Wright et al. (1991), Bennett et al. (1994), and Reach et al. (1995). Puget et al. (1996) used the Pass 3 FIRAS observations to make a tentative background determination similar to one of the methods used here.

At frequencies below $\sim 20 \text{ cm}^{-1}$ ($500 \mu\text{m}$), the FIRB is overwhelmed by the CMB. However, the CMB can be subtracted from the data since its emission is spatially uniform, and it has a Planck spectrum. The dipole anisotropy of the CMB must be included but the other anisotropy is not large enough to be a problem. At frequencies above $\sim 100 \text{ cm}^{-1}$ ($100 \mu\text{m}$), beyond the FIRAS range, the observed spectrum is dominated by the zodiacal emission, which is much more complex, since its intensity and spectrum are spatially varying. In between these frequencies, the observed spectrum is dominated by Galactic emission, which can be identified by its distinct (from zodiacal) spectrum, and its spatial variation over the sky. After the subtraction of these foreground emissions, any isotropic residual emission may still contain a uniform component from the solar system or the Galaxy, which must be estimated and separated from the FIRB. In this paper we examine three methods, which give a consistent result for the FIRB.

2. THE OBSERVATIONS

The FIRAS Pass 4 data consist of spectra between 2 and 96 cm^{-1} (5000 to $104 \mu\text{m}$ wavelength) in each of 6063 pixels on the sky (there are 6144 pixels in the full sky) with 210 frequency bins

per spectrum. They were calibrated using the method described by Fixsen et al. (1994b), with the improvements noted by Fixsen et al. (1996). The Pass 4 FIRAS data have lower noise and lower systematic errors than the previous FIRAS data releases (FIRAS Explanatory Supplement). A weighted average of all of the FIRAS data was used for this analysis. Random uncertainties are ~ 0.05 MJy/sr ($\nu < 50$ cm⁻¹) and up to 2 MJy/sr at $\nu = 90$ for 10% of the sky. Systematic uncertainties are approximately the same magnitude. The small instrumental offsets deduced from the cold external calibrator are what allow this absolute measurement. The instrumental uncertainties are small relative to the uncertainties associated with the foreground removal. We use data from the Diffuse InfraRed Background Experiment (DIRBE) (DIRBE Explanatory Supplement) to sort and analyze the FIRAS data, and to subtract the DIRBE–determined zodiacal dust emission (Kelsall et al. 1998) extrapolated to the FIRAS frequencies, from the FIRAS data.

3. SEPARATION OF THE GALACTIC EMISSION COMPONENT

The infrared (IR) emission from interplanetary dust particles is a minor contributor to the FIRAS emission and then only in the higher (> 70 cm⁻¹) frequency channels. This emission component is removed from the data by using the model developed from the analysis of the DIRBE data (Kelsall et al. 1998). The major challenge facing the search for the FIRB in the FIRAS data is the removal of Galactic emission.

We have used three different and complementary methods for separating the Galactic emission from the FIRB. The first relies on the spatial variability of the Galactic emission component. Assuming a spatially invariant spectral shape (i.e. color) for this component, we use its spatially varying intensity to distinguish it from the isotropic FIRB. The second method uses H I 21 cm and [C II] (157.7 μ m) line emission, which trace the atomic and ionized gas components of the interstellar medium (ISM), as templates for the Galactic emission component. The third method uses the DIRBE 140 and 240 μ m detections of the FIRB (Hauser et al. 1998) to define templates of Galactic emission.

Each of these methods relies on some assumptions, and therefore has its shortcomings. However, the assumptions underlying each method are different, so the similarity between the derived FIRB spectra suggests that this spectrum represents a robust estimate of the FIRB.

3.1. A FIRAS Color Template

The FIRAS sky spectra, $S(\ell, b; \nu)$, are a function of frequency ν and position $\{\ell, b\}$, where ℓ and b are Galactic coordinates. Since the data are binned into discrete pixels, p , and frequencies, ν , we can also write the FIRAS intensity in each pixel as $S_{p\nu}$. As the first step in the analysis we sort the sky into 10 bins. The first bin is the 10% of the sky which is darkest according to the DIRBE 100 μm map, which has had the zodiacal emission removed with the DIRBE zodiacal model. The next bin is the next 10%, etc. Since the DIRBE data are independent of the FIRAS data we have introduced no noise biases by this sorting. Since the amount of FIRAS calibration data is about 10% of the sky data one can think of them as a zeroth bin. Because the calibration uncertainties of the FIRAS data are of the same magnitude as the random uncertainties in 10% of the sky, there is little to be gained by averaging more than 10% of the sky.

We form the average intensity in each bin k , $S_{k\nu}$ ($k = 1, 2, \dots, 10$), using the pixel weights of the FIRAS data. A map of the sky bins is shown in Fig 1. The sorting is primarily based on the intensity of Galactic emission. The resulting spectra are shown in Fig 2a. Several items are apparent from the figure: (1) the CMB radiation dominates below 20 cm^{-1} ; (2) zodiacal emission is evident above $\sim 70 \text{ cm}^{-1}$, especially in the lower intensity bins; (3) between these frequencies the emission is dominated by the Galaxy, which has a similar spectrum in all bins, particularly in the dimmer bins; (4) the [C II] (63 cm^{-1} ; $158 \mu\text{m}$) line is apparent in all spectra; and (5) the [N II] line (48 cm^{-1} ; $205 \mu\text{m}$) line is visible in the brighter bins and the brighter bins have a higher proportion of high frequency radiation (they are warmer). Although noise is evident in the dimmer bins, the signal to noise ratio in the 20 to 70 cm^{-1} frequency interval is good for all bins.

Figure 2b shows the spectra of the bins after the removal of the CMB and the zodiacal dust

emission. The CMB model is made from the low frequency FIRAS data, while the zodiacal model is determined from the DIRBE data (see Kelsall et al. 1998). The zodiacal dust model was interpolated and extrapolated from the DIRBE 240 μm and 140 μm zodiacal models to the FIRAS frequencies, except that for frequencies below 40 cm^{-1} the slope was steepened by multiplying by a factor $(\nu - 20)/20$ for frequencies between 20 and 40 cm^{-1} . Below 20 cm^{-1} no zodiacal correction was made. There is no evidence of zodiacal emission below 20 cm^{-1} in any analysis, so the zodiacal spectrum must steepen between 20 cm^{-1} and 60 cm^{-1} .

The CMB model must be good to more than 3 orders of magnitude for the low frequency Galactic spectra to emerge. The effect of the CMB dipole (also shown in Fig 2a) must also be included in the CMB model. In contrast the zodiacal emission contributes only a small fraction to the emission at frequencies below 80 cm^{-1} , and we can tolerate 20% errors in its estimate.

The spectrum of bin 1 (the faintest 10% of the sky) provides a very robust upper limit on the FIRB. The signal to noise ratio is high and the systematic errors are small relative to the signal. But this is an upper limit, not a detection.

We model the average intensity in each bin as a sum of two components, a uniform component, U , and a spatially varying Galactic component, G , that may be spectrally distinct from U . The average intensity in each bin is then

$$S_{k\nu} = U_\nu + g_k G_\nu, \tag{1}$$

where U_ν is a uniform spectrum containing the FIRB, G_ν is the Galactic spectrum and g_k is a parameter that determines its intensity in the k th bin. There are two degrees of freedom that are unconstrained in this fit. For a given solution (U', g', G') , there exists a family of solutions: $(U' - xG', (g' + x)/y, yG')$ that provide identical fits to $\{S_{k\nu}\}$. The two degrees of freedom are represented by an additive component to the uniform spectrum, and a scaling parameter for the Galactic spectrum. Two additional constraints provide a unique solution to eq. (1). First, the background must be positive, so one solution, U'' is chosen with $x = x_\circ$ so that $U'' = U' - x_\circ G'$ is

at most 2σ negative at any frequency. Second, we scale the Galactic spectrum in terms of its value in the dimmest bin ($k=1$), $G'' = S_1 - U''$. With this choice, the family of solutions is expressed as

$$U = U'' + \gamma G''. \quad (2)$$

The parameter $\gamma < 1$, otherwise the background U is brighter than the intensity S_1 in the dimmest 10% of the sky. Furthermore, $\gamma > 0$, otherwise U falls below the 2σ negative value. We estimate a value of $\gamma \approx 0.2$. A lower value is unlikely because it (weakly) implies a negative background at some frequencies. A higher value unnecessarily ascribes to the background, radiation which is fit equally well with the known Galactic foreground. Also if γ is larger, the Galactic [C II] line is clearly visible in the background spectrum. Nominally the uncertainty in γ would be 0.1 but in view of the systematic nature of the possible errors a σ of 0.2 is appropriate.

Should there be a systematic variation of temperature with intensity it would couple with the assumption of a single color for the Galactic emission leading to errors in the calculated background shape and intensity. Part or all of the “observed” background could be due to this effect for this method.

When small bins are used there is an indication that the temperature is variable, and the temperature depends on Galactic longitude. The spectrum of the Galactic plane is different from that of the high latitude Galaxy, but using the faintest 20 to 80% of the sky gives the same results to a good approximation. The decomposition for the faintest 50% of the sky is shown in Figure 3a. The noise of the FIRAS data increases with frequency and at frequencies $\nu > 80 \text{ cm}^{-1}$ may be affected by zodiacal emission. The feature at $\sim 20 \text{ cm}^{-1}$ is in the low weight data between the low and high frequency channels of the FIRAS and is not significant.

3.2. An H I and [C II] Line Emission Template

The Galactic foreground emission is estimated and removed by subtracting the fraction of the observed emission that correlates with templates of the Galactic IR emission. The H I 21 cm and

[C II] 158 μm lines are good candidates for such templates because they are definitely of Galactic origin, they are both strong, and nearly fully sampled across the sky. While they may not correspond directly to the neutral and ionized gas phases, they are not perfectly correlated with each other and if they are differently associated with the different ISM phases then linear combinations of them could be used to trace the emission of the neutral and ionized gas, the major components that give rise to the high latitude Galactic FIR emission (Reach et al. 1995).

The H I map was used by Puget et al. (1996). We use the AT&T Bell Laboratories H I survey map from Stark et al. (1992) convolved with the FIRAS beam. The [C II] map is from the FIRAS so it already has the right beam profile and sky coverage. We have also tested an [N II] 205 μm template, from the FIRAS data, but at high latitude the [N II] emission is small and there is no significant correlation. For both the H I and the [C II] maps the zero point is not a significant uncertainty. The relation between the line emission and the continuum emission is a far larger uncertainty.

The relation between H I and the IR emission is clearly not linear. At moderate H I column densities the molecular mass fraction of a cloud becomes significant, and IR emission from the molecular gas causes an excess of IR emission over that expected from the H I-IR correlation plot (Boulanger et al. 1996, Spaans & Neufeld 1997). We therefore include a quadratic term in H I in the fit, as well as the [C II] emission as a second tracer. Both line maps are renormalized to an average value of 1 over the faintest half of the sky. The intensity in a given sky pixel is:

$$S_{p\nu} = U_\nu + h_p H_\nu + h_p^2 G_\nu + c_p C_\nu \quad (3)$$

where p is the sky pixel index, h_p is the H I map, c_p is the [C II] map and U, G, H, C are spectra determined from the fit (the U_ν is again the background but not necessarily that of section 3.1).

The linear term is small indicating that the quadratic term absorbs most of the power. Even though the linear term is negative at some frequencies the combination of linear plus quadratic is positive.

We must eliminate the brightest 2/3 of the sky and the south polar region as we have no H I data

with well accurate sidelobe corrections there. These limit the fit to $\sim 25\%$ of the sky in order to get a stable fit. The fit to the [C II] map is quite stable over a wide range of cutoffs but the H spectrum fit, even with the inclusion of the quadratic term, is only stable over the dimmest parts of the sky. The results of the fit are shown in figure 3b.

Since the relation between the H I and the Galactic emission is not linear there is a concern that a quadratic is not the right answer either. Forcing the fit to be linear and cutting enough data to make it fit leaves a very short lever arm for the extrapolation. The [C II] picks up other radiation but there still might be more Galactic radiation not traced by either the H I or [C II].

The expected noise of the fit spectra is evident. This is exaggerated by the high correlation between the h_p and h_p^2 . Still there is a clear signal at lower frequencies.

3.3. A DIRBE 140 and 240 μm Emission Template

In many ways the easiest approach is to use the DIRBE maps and extragalactic background detections at 140 and 240 μm to determine the FIRB from the FIRAS data. Adopting the DIRBE FIRB backgrounds (Hauser et al. 1998) at 140 and 240 μm of 1.17 and 1.12 MJy/sr respectively, we construct Galactic emission templates by subtracting these backgrounds from the zodiacal light subtracted DIRBE maps convolved with the FIRAS beam. This combination has already been shown to model the Galaxy quite well over a large part of the sky (Fixsen et al. 1997a). We represent the pixel intensity at each FIRAS frequency ν in terms of a linear combination of the two DIRBE templates as follows:

$$S_{p\nu} = U_\nu + (D_p^{240} - D_\circ^{240})G_\nu^{240} + (D_p^{140} - D_\circ^{140})G_\nu^{140} \quad (4)$$

where D_\circ^λ and D_p^λ are, the DIRBE background and map intensity at FIRAS pixel p , at wavelength λ . By correlating the FIRAS map to both the 140 and 240 μm DIRBE templates, we allow for temperature variations in the Galactic foreground. The background is obtained by extrapolating the correlations with the DIRBE templates to the DIRBE background values of D_\circ^λ .

Figure 3c presents the results of the fit. To be consistent with the other fits, we plot the results for the dimmest half of the sky. However, the result is very robust and essentially identical results can be obtained for any region of the sky that excludes the Galactic plane.

Of course the uncertainties in the DIRBE FIRB determination at 140 and 240 μm propagate the determination of the FIRB here. We have shown (Fixsen 1997b) that the FIRAS and DIRBE calibrations are consistent, so it is not surprising that the two data sets give consistent results when the amplitude of the background determination for the DIRBE is assumed. The DIRBE maps are only used to determine the *Galaxy* model; the isotropic component need not have been consistent with the FIRAS determination so this method is partially independent.

4. DISCUSSION

The three methods just described have different assumptions, weaknesses and strengths. The first method assumes that the Galactic spectrum is fixed, and that only its intensity varies with position. Temperature variations are observed to occur on various scales (Reach et al. 1995; FIRAS Exp Sup 1997; Lagache et al. 1998). Based on the DIRBE analysis, we expect these variations to have a only a small effect on our results. The DIRBE high latitude data at 240 μm were analyzed using both a single- and a variable-spectrum model to describe the Galactic foreground emission (Arendt et al. 1998), with no significant difference in the derived background.

The second method does not assume a fixed Galactic spectrum, but almost all of the power in the fit is in a single component indicating that there is little systematic correlation of temperature with intensity of the H I 21 cm line. This method solves directly for the dust emission from the dominant neutral and ionized phases of the ISM. It therefore avoids a potential problem of the third method (which relies on the DIRBE analysis) using backgrounds derived from the IR-to-H I correlation only. Two problems with this method are, that at the FIRAS resolution, the correlation between the IR and the H I line intensity is non-linear and that it ignores the molecular regions. The first was treated by using a quadratic fit to the relation. This choice is not

unique, but it is supported by observations of the IR to H I correlation in the Galaxy (Dall’Oglio et al. 1985; Reach, Koo, & Heiles 1994). Molecular clouds are less abundant at the high Galactic latitudes that are used here.

The third method relies on the accuracy of the DIRBE determination of the FIRB. The main uncertainty in the background determination are those associated with the determination of the foreground emission, and they are discussed in detail by Hauser et al. (1998). The use of a DIRBE template for the FIRAS background determination introduces another uncertainty, namely the consistency between the FIRAS and DIRBE calibration. Fixsen et al. (1997b) show that the most significant difference in the calibration is in the 240 μm DIRBE band, but using the FIRAS instead of the DIRBE calibration for that band introduces a very small change in the background, from a value of 13.6 to 12.7 $\text{nW m}^{-2} \text{sr}^{-1}$ (Hauser et al. 1998).

Overall, the three methods yield a consistent spectrum for the FIRB, an encouraging result considering the substantial differences in the three approaches (see fig 4a). The weaknesses of each method are compensated by the other methods. The color method assumes a single spectrum, but the other methods allow for color variation in the Galactic foreground. The line emission method uses a quadratic fit over 25% of the sky, but the other methods use linear fits which are insensitive to the fraction of sky. The DIRBE method only uses the correlation between H I and the foreground in small regions, but the line emission method includes ionized gas and the color method makes no assumptions about the gas.

In all three FIRB spectra the background peaks at $\sim 50 \text{ cm}^{-1}$ ($\sim 200 \mu\text{m}$), and exhibits a definite turnover at the higher frequencies. The higher frequencies are more affected by both noise and systematic effects. The average of the three spectra can be fit by:

$$I_\nu = (1.3 \pm 0.4) \times 10^{-5} (\nu/\nu_0)^{.64 \pm .12} P_\nu(18.5 \pm 1.2 \text{ K}), \quad (5)$$

in the 5 to 80 cm^{-1} frequency range (λ between 125 and 2000 μm) where $\nu_0 = 100 \text{ cm}^{-1}$, and P_ν is the familiar Planck function. The uncertainties are highly correlated, with correlations of .98

for the intensity and index, $-.99$ for the intensity and temperature. and $-.95$ for the index and temperature.

Figure 4b compares the analytical fit to the FIRB derived here, to the tentative background derived by Puget et al. (1996). The spectra differ significantly at $\nu \sim 35 - 60 \text{ cm}^{-1}$, probably the result of the difference in subtraction of dust emission related to H^+ . The crosses in the Figure represent the nominal DIRBE detections at 140 and $240 \mu\text{m}$, while the diamonds represent the DIRBE detections using the FIRAS calibration. While the effect of the FIRAS calibration is larger at $140 \mu\text{m}$, the uncertainty in the calibration is larger at this wavelength. So, the FIRB derived here is consistent with that derived by the DIRBE, within the uncertainty of the DIRBE–FIRAS calibration. The range of values for the FIRB at $100 \mu\text{m}$ represent the upper limit derived by Kashlinsky, Mather, & Odenwald (1996) from a fluctuation analysis of the $100 \mu\text{m}$ DIRBE maps and the lower limit is derived by Dwek et al. (1998) from the 140 and $240 \mu\text{m}$ DIRBE detections.

Dwek et al. (1998) show that the uniform DIRBE residuals cannot be produced by any local (solar system or Galactic) emission sources. Hence, the uniform residual derived here is most likely of extragalactic origin. The total flux received in this wavelength region is $14 \text{ nW m}^{-2} \text{ sr}^{-1}$, or about 20% of the total expected flux of about $70 \text{ nW m}^{-2} \text{ sr}^{-1}$ associated with the production of metals throughout the history of the universe in some models (Dwek et al. 1998).

We thank the many people involved in processing the FIRAS data. We thank the DIRBE team for helpful discussions and the zodiacal model, G. Hinshaw for help in producing the plots, and the referee, W Reach for his helpful comments. This work was supported by the Office of Space Sciences at NASA Headquarters.

REFERENCES

- Arendt, R. et al., 1998, ApJ,
- Bennett, C. L. et al., 1994, ApJ, 436, 423
- Bennett, C. L. et al., 1996, ApJ, 464, L1
- Boggess, N. W. et al., 1992, ApJ, 397, 420
- Boulanger et al., 1996, A&A, 312, 256
- COBE Diffuse Infrared Background Experiment (DIRBE) Explanatory Supplement, 1997, ed. M. G. Hauser, T. Kelsall, D. Leisawitz, and J. Weiland, COBE Ref. Pub. No. 97-A (Greenbelt, MD: NASA/GSFC), available in electronic form from the NSSDC.
- COBE Far Infrared Absolute Spectrophotometer (FIRAS) Explanatory Supplement, 1997, ed. S. Brodd, D. J. Fixsen, K. A. Jensen, J. C. Mather and R. A. Shafer, COBE Ref. Pub. No. 97-C (Greenbelt, MD: NASA/GSFC), available in electronic form from the NSSDC.
- Dall’Oglio, G., de Bernardis, P., Masi, S., Melchiorri, F., Moreno, G., & Trabalza, R. 1985, ApJ, 289, 609
- Dwek, E. et al., 1998, ApJ, submitted
- Fixsen, D. J. et al., 1994a, ApJ, 420, 445
- Fixsen, D. J. et al., 1994b, ApJ, 420, 457
- Fixsen, D. J. et al., 1996, ApJ, 473, 576
- Fixsen, D. J. et al., 1997a, ApJ, 486, 623
- Fixsen, D. J. et al., 1997b, ApJ, 490,482
- Hauser, M. G. et al., 1998, ApJ, submitted
- Kashlinsky, A., Mather, J. C., & Odenwald, S. 1996, ApJ, 473, L9
- Kelsall, T. et al., 1998, ApJ, submitted
- Lagache, G. et al., 1998, A&A, in press

Mather, J. C. et al., 1990, ApJ, 354, L37

Mather, J.C., Fixsen, D.J. and Shafer, R.A. “Design for the COBE Far Infrared Absolute Spectrophotometer (FIRAS),” COBE Preprint 93-10, Proc. SPIE, vol 2019, pp. 168-179, conf. on Infrared Spaceborne Remote Sensing, in San Diego, CA, 11-16 July 1993, (SPIE: Bellingham, WA)

Mather, J. C. et al., 1994, ApJ, 420, 440

Spaans, M. & Neufeld, D. 1997, ApJ, 484, 785

Puget, J. L. et al., 1996, AA, 308, L5

Reach, W. T., Koo, B. -C., & Heiles, C. 1994, ApJ, 429, 672

Reach, W. T. et al., 1995, ApJ, 451, 188

Stark, et al., 1992, ApJ Sup, 79, 77

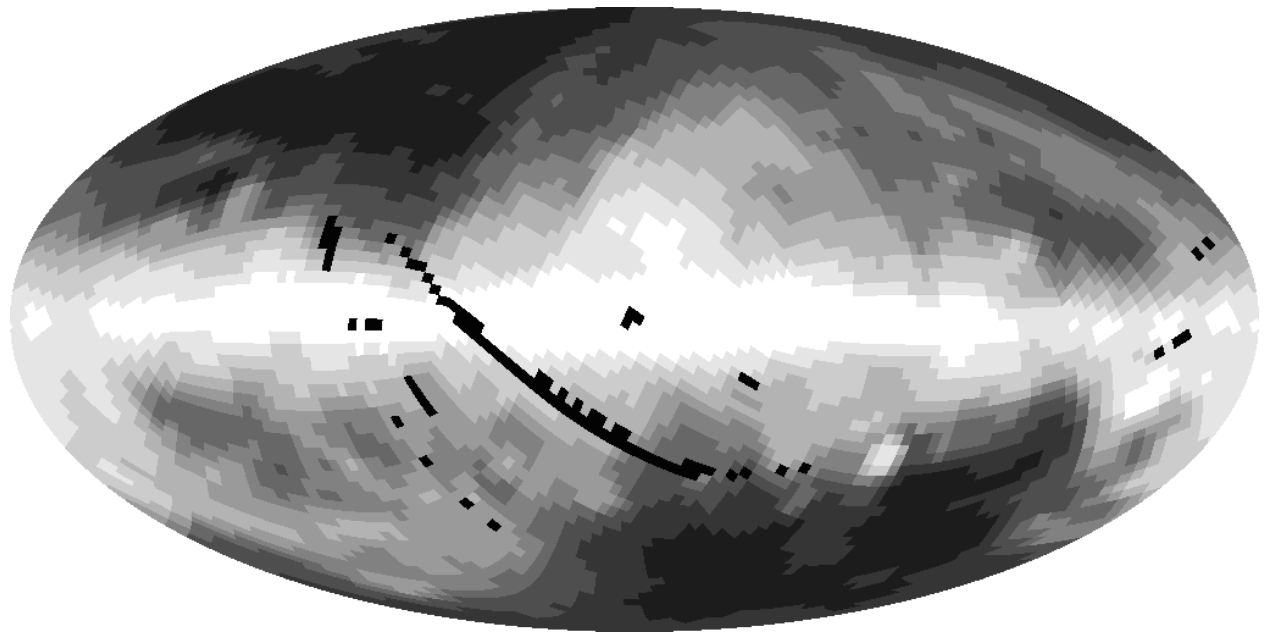
Wright, E. L. et al., 1991, ApJ, 381, 200

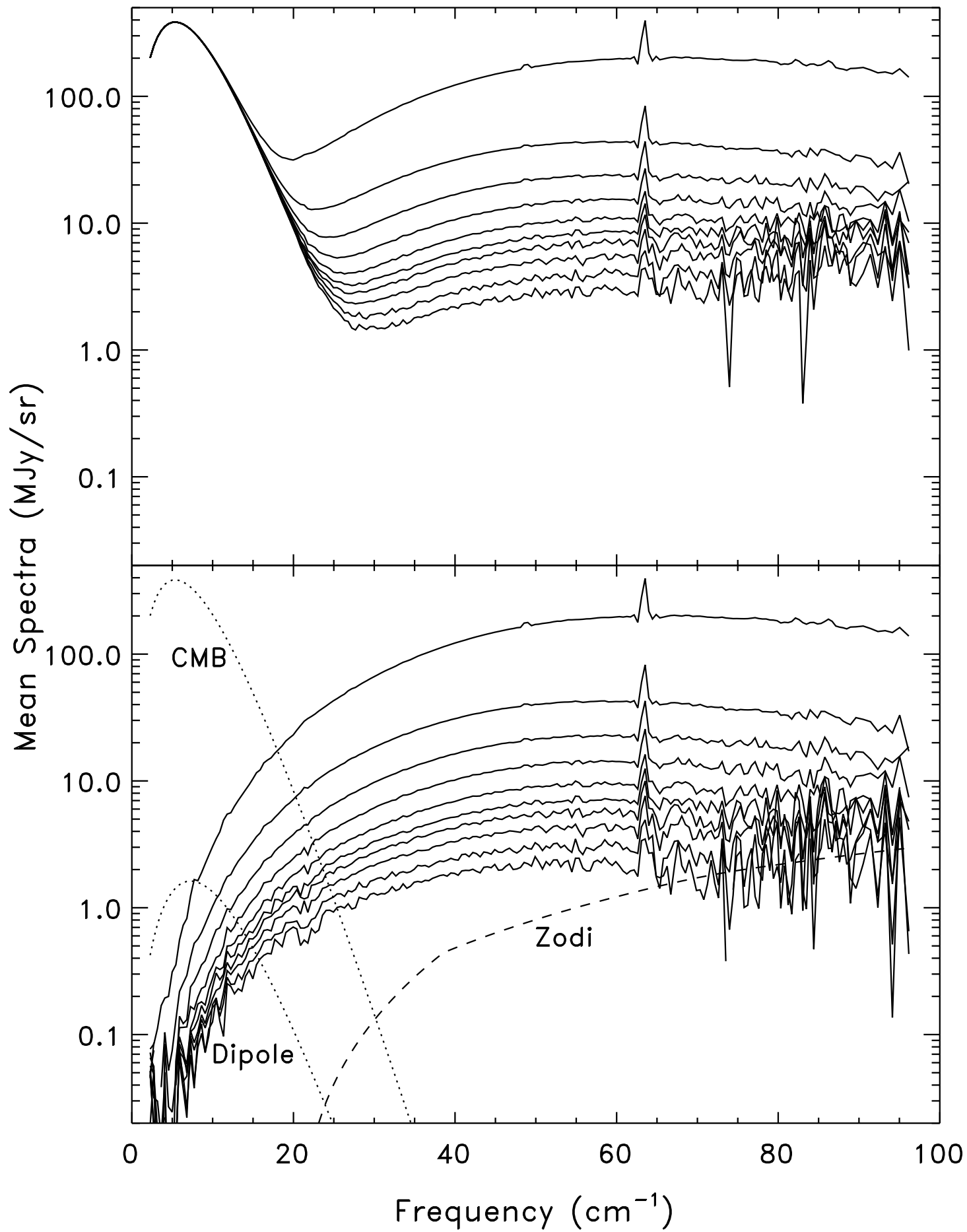
Fig. 1.— Ten regions of the sky as defined by the DIRBE 100 μm intensities. The brightest region is white. The black streak and spots are pixels not used in this analysis.

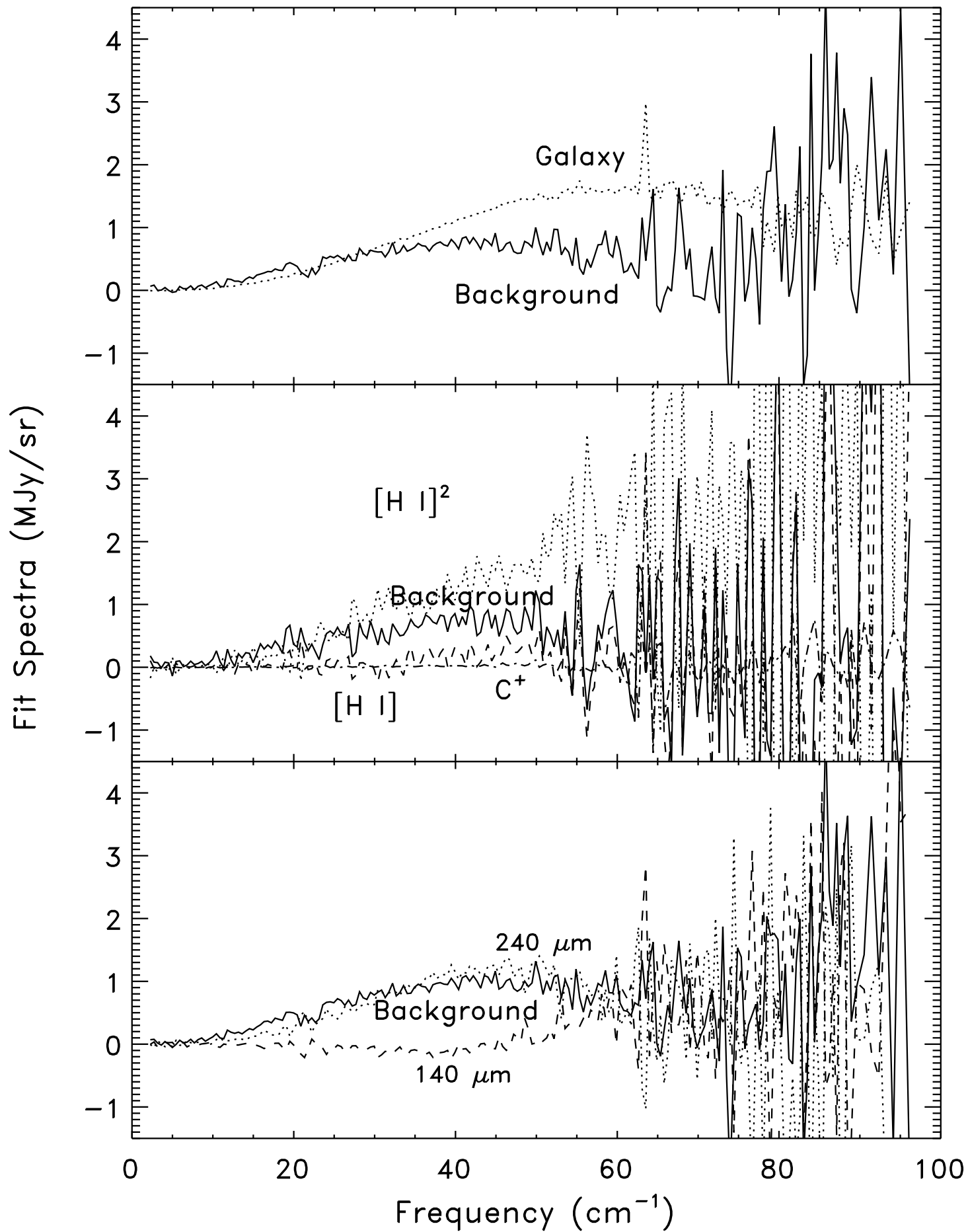
Fig. 2.— a) Average spectra for the ten regions shown in Figure 1. b) The spectra after the removal of the CMB and the zodiacal emission models. The CMB and CMB dipole are shown with dotted lines and the average zodiacal emission is shown with a dashed line.

Fig. 3.— a) Galaxy (dotted) and minimum background (solid) spectra determined from method 1 (§3.1). b) The background U and the spectra C , H , and G derived by using the H I and [C II] line emission maps to fit the FIRAS data [eq. (3)]. The line maps have been normalized to 1 over the dimmest half of the sky. The background is given by a solid line, the dotted line is C , the dashed one is the H , and the dash-dotted line is G (see §2.2 for more details). c) The background derived by using DIRBE 140 and 240 μm Galactic templates. The solid line is the background, and the dashed and dotted lines are the spectra associated with the 240 and 140 μm Galactic templates. Although the 140 μm spectrum is negative there is enough 240 μm emission to make the Galaxy model positive everywhere.

Fig. 4.— a) A comparison of the background spectra derived by the three different methods. The solid line is the color model (§ 3.1), the dotted line is the H I-[C II] model (§ 3.2), and dashed the line is the DIRBE model (§ 3.3). The smooth curve is $1.3 \times 10^{-5}(\nu/\nu_o)^{.64}P_\nu(18.5 \text{ K})$, where $\nu_o = 100 \text{ cm}^{-1}$ and P is the Planck function. b) A comparison of the average background spectrum derived in this paper (given by its analytical representation, solid line) with the DIRBE determination (crosses) at 140 and 240 μm (Hauser et al. 1998), and the range of allowable 100 μm intensities (Dwek et al. 1998). The diamonds are the DIRBE determinations recalibrated with the cross calibration in Fixsen (1997b). The light lines represent 1σ errors on the derivation. Also shown is the tentative determination of the background by Puget et al. (1996) with (dashed line) and without (dash triple dot line) their H^+ correction.







Wavelength (μm)

1000

100

I_ν Background (MJy/sr)

1.0

0.1

νI_ν Background ($\text{nW}/\text{m}^2/\text{sr}$)

10.0

1.0

0.1

10

Frequency (cm^{-1})

100

